投稿論文(英文)
PAPER

J. Geotech. Eng., JSCE, No. 554/III-37, 1-17, 1996 December

LIQUEFACTION SHAKING TABLE TESTS FOR SANDY GROUND WITH EMBANKMENT

Hiroshi ABE[1]

[1]Member of JSCE, Dr. Eng., Professor, Dept. of Civil Eng., Gunma College of Technology
(580, Toriba-machi, Maebashi, Gunma 371, Japan)

This paper tries to examine the dynamic behavior of earth-structure as a ground with embankment during liquefaction and assess the effectiveness of the liquefaction countermeasures. From a total of six types of shaking table tests it can be seen that even for soft sandy ground liable to give rise to liquefaction in the surrounding horizontal ground parts, the excess pore water pressure of the foundation ground directly below the embankment did not reach the effective overburden stress and liquefaction did not occur. With a two-dimensional direct non-linear liquefaction program using effective stress analysis, it was possible to reproduce the measurement results obtained in the shaking table tests.

Key Words : *liquefaction, sandy ground, embankment, shaking table test, two-dimensional effective stress analysis, direct non-linear method*

1. INTRODUCTION

The author is in the process of developing the TOTAL[1)] system, an evaluation system designed primarily for the assessment of the seismic resistance of civil engineering structures. This development is carried out with a view to streamlining the anti-liquefaction measures for earth-structures.

The general outline of the TOTAL is shown in **Figure 1**. In the establishment of the system, allowance was made for the fact that the information of liquefaction damage in Tokyo has been extremely minor so that the system preparation work involved, in the first stage, (1) establishment of a liquefaction analysis program based on effective stress method, (2) carrying out of model shaking table tests, and (3) collecting and systematically ordering of information from studies of ground and earth-structure. In the second stage, the work involved a comparison of the analytical results of (1) and the experiment results of (2) so as to ascertain the performance capability and the suitability range of the analysis program. In the third stage, the task was to create a system capable of reproducing the cases of damage under (3) (precedents) from the analyzing program under (1). After this, the analysis was performed with the data

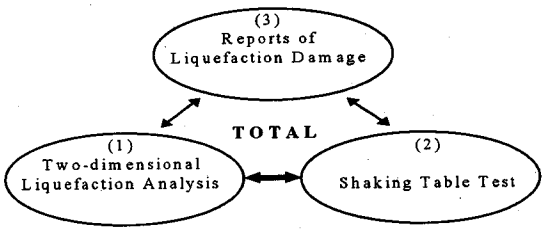

Fig.1 General outline of the TOTAL

for the existing earth structures and foundation grounds under the control of the Metropolis of Tokyo to establish a system for predicting liquefaction damage and for examining appropriate preventive measures.

This paper describes the results of shaking table tests[2)] performed on embankment models in a 1g gravitational field with a view to confirming the effectiveness of the anti-liquefaction measures which have been implemented as an integral part of the present research project. This paper also presents the simulation results for the shaking table tests on a ground with embankment using the program[3)] for two-dimensional direct non-linear liquefaction analysis based on the effective stress method

obtained in the second stage of the system construction work.

2. SHAKING TABLE TEST[4)]

(1) Experimental method

A total of six types of models referred to as Case-1 through Case-6 are shown in **Figure 2**. Used for the shaking table tests was a soil container with a pile of 18 aluminum frames capable of horizontal displacement of the side walls in the direction of vibration. The dimensions of the soil container with the stacked frame apparatus were an internal length in the direction of vibration of 350cm, a width of 80cm, and a depth of 100cm.

The foundation grounds for the above models were prepared by using Toyoura standard sand (Specific gravity of soil particles: G_s=2.645, Maximum dry unit weight: $\gamma_{d,max}$ =1.660g/cm^3, Minimum dry unit weight: $\gamma_{d,min}$=1.356g/cm^3, Mean grain size: D_{50} = 0.198mm). Except for Case-2, all other five models were prepared on the assumption of a saturated soft sandy ground and the foundation ground was made by controlling the air-pluviation height of the dry Toyoura sand in such a manner that its relative density *Dr* was approximately 60%. The *Dr* values shown in **Fig. 2** represent the measurement data prior to the shaking. For the Case-2 model, a dense ground was assumed and the foundation ground prepared in such a manner that its *Dr* was 96% (the target *Dr* value was 80%).

As an example of the law of similarity we have chosen the research results obtained by Clough and Pirtz[5)] and which can be applied to the large shear strain amplitude range. All models had a foundation ground layer thickness of 70cm. The layer thickness for the foundation ground was determined on the basis of the similarity law by allowing for the limitations imposed by the dimensions of the soil container and the fact that the thickness of the alluvial sand layer (Yurakuchosou-jyoubu) in the Tokyo Lowland is in the order of 10m maximum. The "model" referred here, however, does not signify a specific object to which the law of similarity has been supplied as being a real structure such as a prototype embankment. In the strict sense, the term model is used here in the sense that it is a small real object on which tests and analyses have been performed. The results of these tests and analyses are reported below.

The purpose of the experiments below was to investigate the dynamic behavior of the

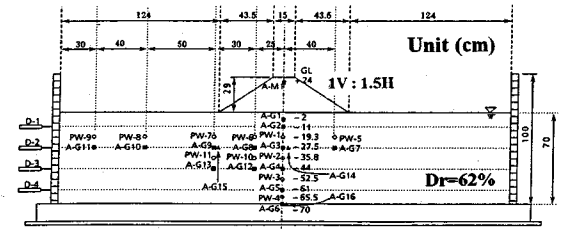

Case-1 unimproved ground

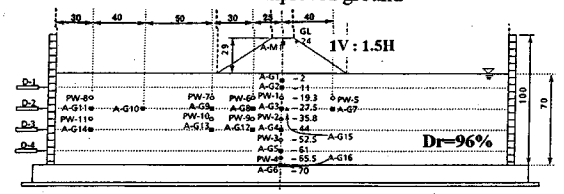

Case-2 improved ground (compaction)

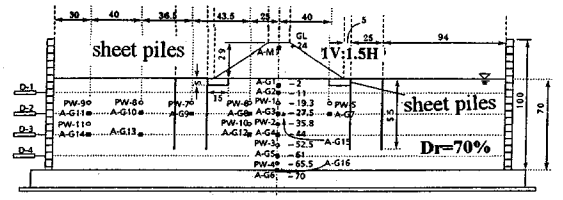

Case-3 improved ground (double sheet piles)

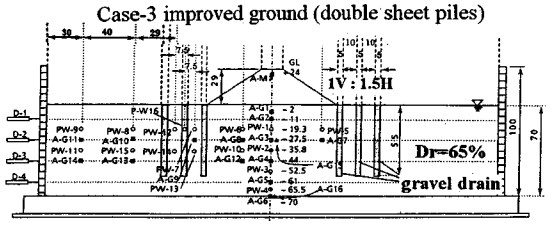

Case-4 improved ground (gravel drain)

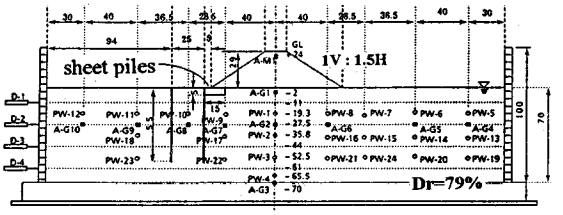

Case-5 improved ground (one side double sheet piles)

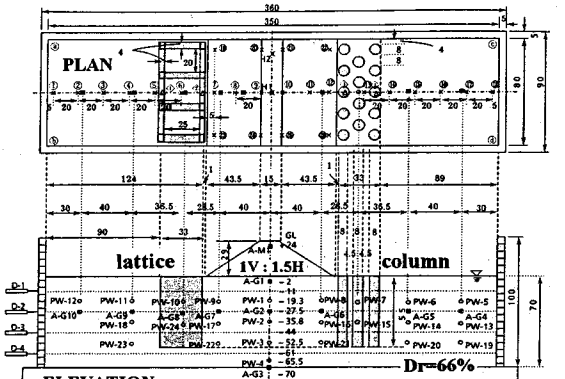

Case-6 improved ground (deep mixing)

⟹ Displacement transducer ■ ▲ Accelerometer ○ Pore pressure gauge

Fig. 2 Experimental models

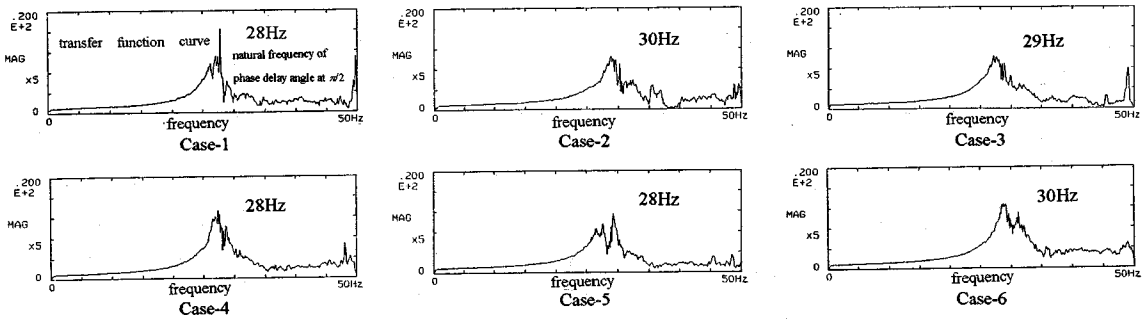

Fig. 3 Ground's transfer function curve and natural frequency of phase delay angle at $\pi/2$

foundation ground directly beneath the embankment (being equivalent to a condition in which liquefaction can take place on level ground) and of the peripheral parts surrounding the embankment structure when a seismic input acceleration is applied whose magnitude is such that liquefaction phenomena can occur on level non-improved ground. The Case-1 test was performed using a model with the embankment heaped on a sand foundation. This model was considered as an embankment model on standard soft ground. The Case-2 test was performed using a dense sand foundation model on the assumption of a compaction method being applied. The Case-3 test was performed by modeling a condition in which a double sheet piles were placed at the toe of the slope of the embankment on a soft sandy ground. In this test, two aluminum sheets (3mm thickness, 79cm width, and 55cm depth) were positioned at a spacing of 25cm in such a manner that the sheets had a clearance of 5cm from the toes of the embankment on either side. The sheets were fastened only at the top using nine aluminum rods. The Case-4 test was performed by modeling a condition in which a gravel drain was located at the toes of the embankment on a soft sandy foundation. The drain material consisted of gravel of 2 - 3mm grain diameter (Mean grain size: D_{50} = 2.17mm). Three rows of such gravel drains were arranged in the form of 5cm thickness, 80cm width, and 55cm depth wall-type improvement structures spaced at a pitch of 10cm from the toes of the embankment on either side. The Case-5 test was performed by modeling a condition in which a double sheet piles was placed on one side of the toe of the embankment on a soft sandy ground. In this test, the sheet pile used in Case-3 was re-used. The Case-6 test was performed by modeling a condition in which a deep mixing method of soil stabilization was applied at the toes of the embankment on a soft sandy ground. For the deep mixing improvement, a lattice and column type pure concrete (Unit weight: 2.3gf/cm^3) was used. The lattice type improvement with a length 33cm, a width of 76cm, a depth of 55cm, and a wall thickness of 4cm was placed at a distance of 1cm from the embankment (Improvement ratio: 38%). The column type improvement was arranged in three zigzag rows of a total of 14 columns, having a diameter of 8cm and a depth of 55cm (Improvement ratio: 27%). As can be seen in **Fig. 2**, the bottom sections of the improvement structures were secured in the loose sand foundation but not fastened on to the base of the soil container. This was due to the fact that the soft alluvial silt layer (Yurakuchosou-kabu) of the Tokyo Lowland is extremely thick. After the foundation ground had been prepared, the soil container was transferred on to the shaking table and the air in the foundation ground was expelled and replaced by CO_2, with subsequent injection of water from the bottom of the soil container until the foundation was saturated. In order to prevent the water contained in the foundation ground from seeping into the embankment during vibration, a loosened vinyl sheet had been laid previously in the position of the embankment. Two Teflon® sheets were attached to the rubber membrane on the side surface of the soil container to minimize friction between the embankment and the side walls of the soil container.

An embankment consisting of unsaturated Toyoura sand was heaped on the foundation ground. The embankment was shaped by hand. The embankments for all of the six model cases were made on a scale corresponding to a height of 29cm, a width of 80cm, a crest width of 15cm, and a gradient of slope of 1V:1.5H.

Using the microtremor method, the natural frequency of the model ground was determined by the transfer function curve and the phase angle at $\pi/2$ obtained from the phase delay curve between the surface of grounds and the base of the container. All transfer function curves obtained by the tests are shown in **Figure 3**. The graph does show a natural

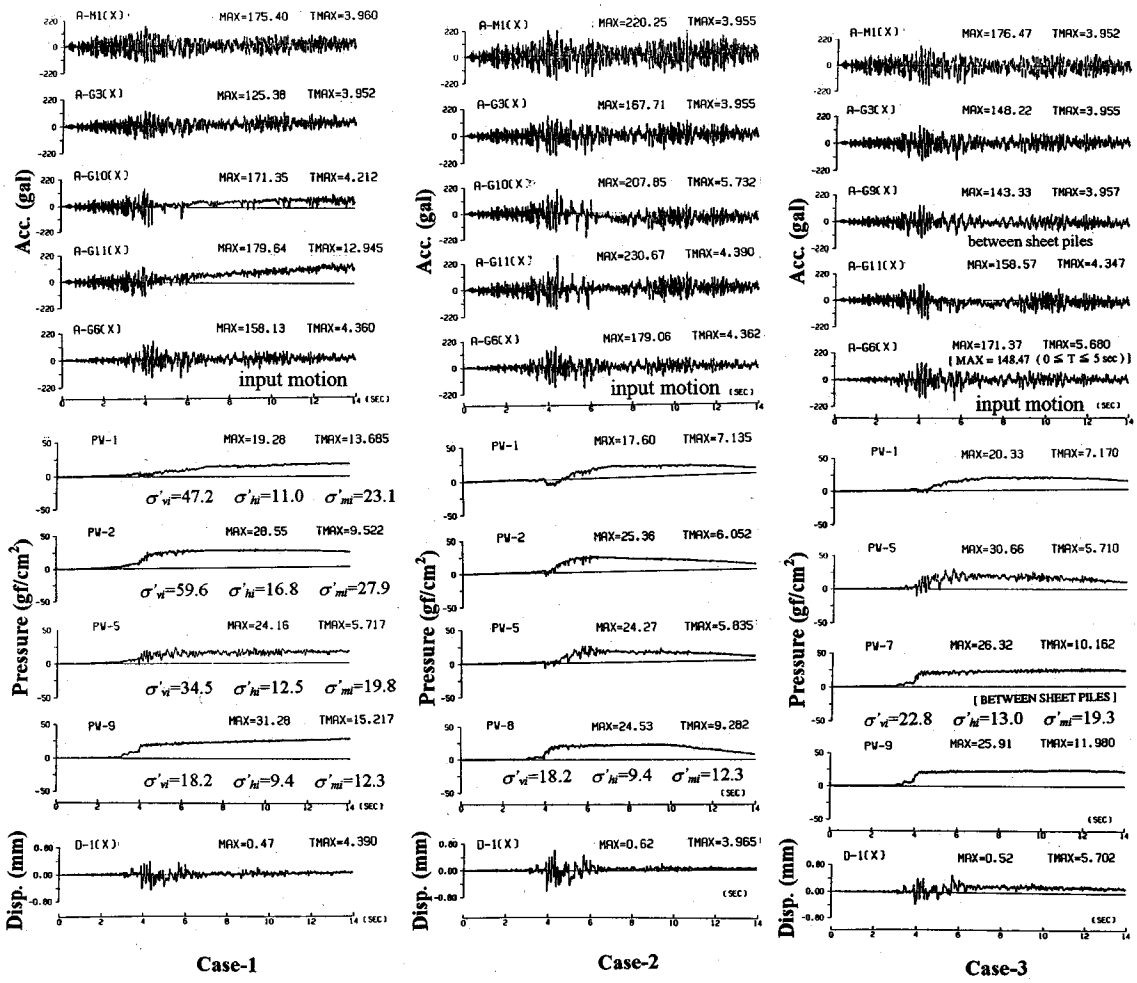

Fig. 4a Observed acceleration, excess pore water pressure, and displacement time histories (Case 1, 2, and 3)

frequency for the phase angle at $\pi/2$. **Fig. 3** indicates that the natural frequency for the dense-ground case (Case-2) and the case of a concrete-containing ground (Case-6) can be seen as being 30Hz. In other cases, the natural frequency was slightly lower than this, with values in the range of 28 - 29Hz.

Used for the shaking table tests was the 4m × 4m three-dimensional shaking table owned by the Institute of Technology, Shimizu Corporation. The shaking table was designed to have only one direction of vibration, which is in the longitudinal direction of the soil container. The acceleration wave form used for the tests was the Akita-S N-S wave[6] recorded during the Nihonkai-chubu Earthquake which occurred on May 26, 1983. This wave form is preserved by the Akita city branch office of the Ministry of Transport. The time scale factor by considering the law of similarity[5] was condensed to 1/4(similarity ratio; model/prtotype=$1/\lambda^{0.5}$,λ=16). The duration of the shaking was 14 seconds.

The tests were carried out in the following procedure. Initially, vibration was performed, in all test cases, at a rate of about 80gal maximum input acceleration, a level of vibration described as medium-scale, to examine the behavior of the embankment and foundation ground immediately prior to liquefaction. Next, the water which had accumulated on the soil surface was drained off to proceed to a shaking test at a maximum acceleration of 160 - 170gal, a level of vibration described as the liquefying vibration. Finally, post-liquefaction tests were performed on each and all models using a maximum acceleration of around 300gal for re-liquefaction.

(2) Test results and discussions

Figure 4 gives primary examples showing the time histories of the acceleration and excess pore

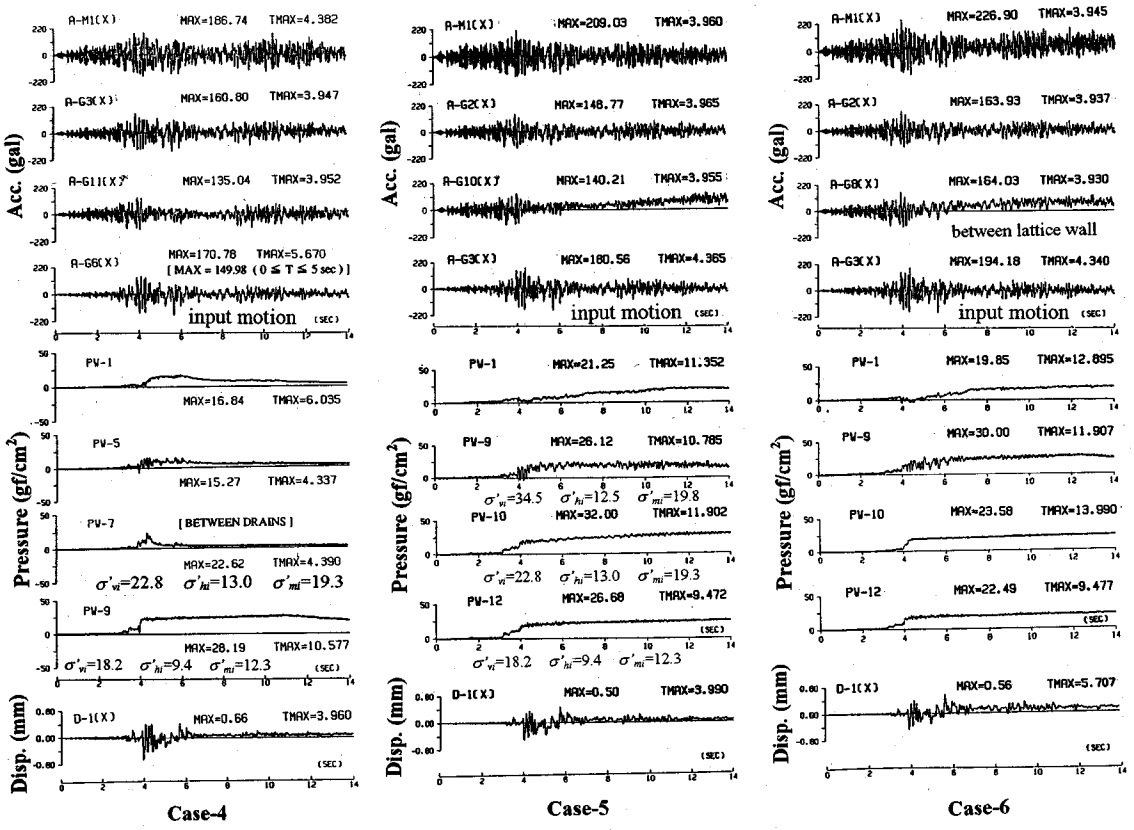

Fig. 4b Observed acceleration, excess pore water pressure, and displacement time histories (Case 4, 5, and 6)

water pressure (E.P.W.P.) measured for all models during the liquefying vibration tests. The observed maximum input acceleration amplitudes (0≤t≤5sec) for the liquefying vibration were 158gal in Case-1, 179gal in Case-2, 148gal in Case-3, 150gal in Case-4, 181gal in Case-5, and 194gal in Case-6. While the maximum amplitudes were somewhat small in Cases-3 and -4, it is believed that the shaking tests were accomplished under roughly the same condition.

The effective confining stresses (initial effective vertical stress: σ'_{vi}, initial effective horizontal stress: σ'_{hi}, and initial effective mean stress: σ'_{mi}) shown in **Fig. 4** were determined by the linear elastic self-weight analysis using FEM modeling for the Case-1 model shown in **Fig. 2**. The graphs without initial stress indication have the same values as those for the measurement points of Case-1. In the analysis, Young's modulus was taken as $E = 7.4\times10^4$ gf/cm^2 and Poisson's ratio as $\nu = 0.3$, with submerged unit weight being $\gamma' = 0.95$gf/cm^3 for the sandy ground and $\gamma' = 1.05$gf/cm^3 for the gravel. For the unsaturated embankment soil, however, wet unit weight was taken as being $\gamma_t = 1.45$gf/cm^3. Young's modulus was determined from the natural frequency value obtained in the shaking table tests that were performed as preliminary tests.

In all cases shown in **Fig. 4**, including the unimproved sandy ground of Case-1, the acceleration response wave form in the center of embankment was observed to follow the input wave form, without any evidence of a trend toward longer periods and wave form loss during liquefaction. Near the surface of the horizontal ground (e.g. A-G11(X) in Case-1), however, the acceleration was observed to become extremely small, with the period lengthening. The period was also observed to lengthen for the acceleration between the sheet piles of Case-3 and between the lattice-type improvement structures of Case-6.

Figure 5 shows the maximum acceleration amplitude distribution with depth in the center of the embankment. As can also be recognized from **Fig. 5**, the acceleration amplitude decreased in the near-medium depth range of the foundation ground. More than the liquefying vibration amplitude, this may be attributed to the apparent non-linear elasticity of the sandy ground.

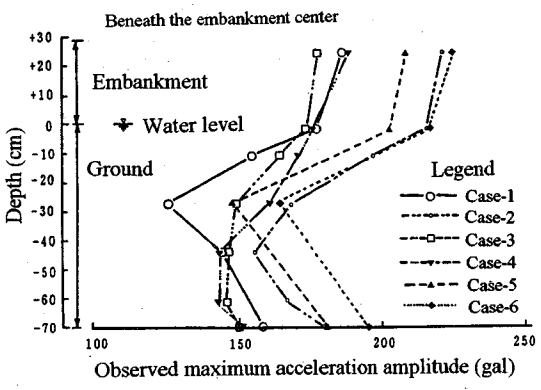

Fig. 5 Maximum acceleration amplitude

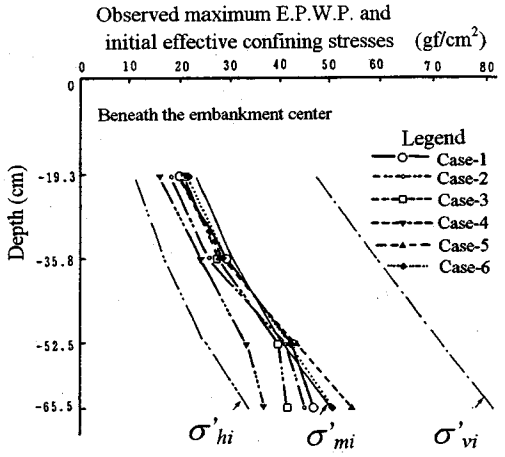

Fig. 6 Maximum excess pore water pressure

From the time histories for the excess pore water pressure in Case-1 shown in **Fig. 4**, it can be seen that the water pressure generally begins to increase after vibration for 3 seconds. Immediately after 4 seconds, the increase in excess pore water pressure tends to be very dramatic. In Case-2, however, there was only a small increasing trend. In the same time, Case-4 showed a rapid decrease in excess pore water pressure due to the dissipation effect of the gravel drain on the excess pore water pressure. The input acceleration wave form shown in **Fig. 4** suggests that the dominant acceleration range, including the maximum amplitude, starts to emerge from around 4 seconds. This clearly indicates that the rise in excess pore water pressure is influenced by the input acceleration amplitude. Directly below the embankment center, the water pressures of shallow foundation point continued to increase in Cases -1, -3, -5, and -6 also after around 6 seconds after the appearance of the dominant acceleration amplitude.

Comparison of the excess pore water pressures below the embankment center and under the slope, both at the same depth, shows that in Cases -1 and -2 without improvement structures at the toes of the embankment, the water pressure of the foundation under the slope was greater than the water pressure immediately below the center of the embankment.

In Case-3 with double sheet piles improvement expected to produce a lateral confining effect, it was found that the excess pore water pressure beneath the embankment was greater than in the other test cases. It was also found that the water pressure increased to a level equal to the initial effective vertical stress σ'_{vi} in the foundation ground between the sheet piles of Case-3 and the lattice-type improvements of Case-6, resulting in liquefaction. The foundation between the gravel drains of Case-4, however, exhibited only a momentary increase in excess pore water pressure which was dissipated immediately afterwards. In the horizontal foundation part (e.g. pw-9 in Case-1, 3, and 4) removed from the embankment, however, it was possible to confirm in all tests that the excess pore water pressure reached the initial effective vertical stress σ'_{vi} and that liquefaction did occur.

Figure 6 shows the depth distribution for the maximum excess pore water pressure beneath the center of the embankment. From **Fig. 6** it can be seen that the maximum excess pore water pressure becomes greater than the initial effective horizontal stress σ'_{hi} in the area beneath the center of the embankment, without reaching the initial effective vertical stress σ_{vi}. Rather, it remained within the range of the initial effective mean stress σ'_{mi}. The results of two-dimensional self-weight analysis have demonstrated that the ratio of the initial effective horizontal stress σ'_{hi} to the initial effective vertical stress σ'_{vi} is smaller than the coefficient of earth pressure at rest K_0. Beneath the embankment, it may be assumed that the lateral confining effect is not strong as in the horizontal ground portion. It may therefore be concluded that liquefaction does not occur because the effective normal stress σ'_n on plane subject to the action of dynamic shear stresses τ_d does not become zero, with the foundation retaining its rigidity[7]. It is believed that the fact that the response acceleration wave-form beneath the embankment did not show any tendency for the period to lengthen as shown in **Fig. 4** is due to this phenomena.

In addition, **Fig. 4** shows the horizontal

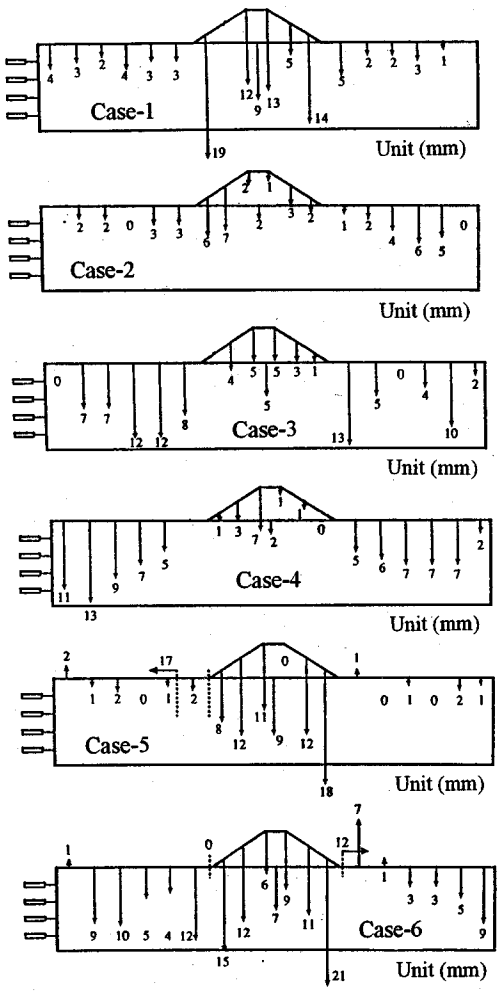

Fig. 7 Displacements after experiments

displacement time history on the side wall of shaking container. After the experiments, the maximum response displacement values at point D-1 were found to have roughly the same values even though they differ. The results likely to account for this are that as a common feature for all cases under study, a non-liquefaction layer may form immediately underneath the embankment and also because the value shows the mean displacement for the soil container as a whole.

3. EFFECTIVENESS OF SOIL IMPROVEMENT

Figure 7 shows the vertical displacement of the embankment and the ground surface after liquefying vibrations. For a loose sandy foundation ground, it

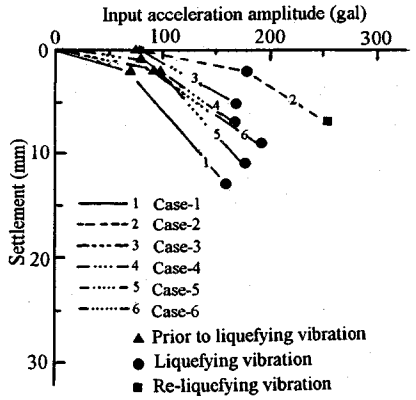

Fig. 8 Relation between settlement of embankment crest and input acceleration amplitude

can be seen that the embankment in Case-1 exhibits a dramatically large amount of settlement whereas the embankments of Cases -3 and -4 show only a small amount of settlement. In the horizontal ground parts it can be seen that except for Case-2 the improved grounds show a larger amount of settlement than the unimproved ones. The reason why the embankments of Cases -5 and -6 have an unexpectedly large amount of settlement may be seen as being due to the left/right non-symmetrical improvement adopted for these embankments.

Figure 8 shows the input acceleration amplitude and the settlement of the embankment crest. It can be seen from this figure that in all experimental cases the amount of embankment crest settlement was found to increase with increase in the input acceleration amplitude. In Case-2 (compaction method), however, it was found that the amount of settlement of the embankment crest was significantly lower than for any of the other cases.

All of the tests have demonstrated that the grounds below the embankments are easily deformed in lateral direction as a result of liquefaction having occurred in the horizontal ground portion. Since there are no structures confining the deformation to the sides in the non-improved foundation of Case-1, it is logical that the embankment showed a large amount of settlement. The reason why the horizontal foundation recorded a small amount of settlement is due to the fact that the surrounding foundation was raised under the influence of the lateral flow. In contrast, it was found in Case-3 that the settlement of the embankment was contained because the lateral flow was confined by the sheet pile improvement structures. When Case-5 with sheet pile improvement on one side is compared with Case-3 with improvement on both sides, it can be seen that the former has a lager amount of embankment

settlement. The reason may be seen as being due to the occurrence of lateral flow on the non-improved side. This suggests that non-symmetrical anti-liquefaction measures appear to have little effect on the prevention of liquefaction.

While liquefaction was impeded and lateral flow contained by the gravel drain improvement in Case-4, the horizontal foundation showed a large amount of settlement under liquefaction.

The column type improvement using deep mixing method in Case-6, exhibited horizontal collapse, with the column top moving 12mm to the side of the horizontal foundation while the lattice type improvement showed no such movement. The displacement of the embankment is governed by the behavior of the different forms of improvement. In the case of a column type improvement, it can be seen that there is a large amount of settlement at the tow of the embankment on the improvement side but little settlement of the horizontal ground as a result of the lateral flow.

With the dense foundation of Case-2, however, it was found that while the maximum excess pore water pressure was roughly equal to that of the soft sandy ground, the embankment and the ground surface exhibited little settlement. Dense compaction of the soft foundation is capable of containing the extent of deformation in the embankment and the foundation so that such compaction may be considered an effective measure of controlling liquefaction. Generally, compaction of the foundation ground tends to give rise to vibration and noise so that consideration must be given to the environment in which the compaction work is executed. In overcrowded city areas, the choice of construction method is a major factor in site environment control so that the construction method has to be carefully selected, it cannot be selected in a random manner.

4. ANALYTICAL METHOD

(1) Liquefaction analysis

This section shows an outline of the newly developed EFFCTD program for liquefaction analysis. The program permits seismic response analysis using direct integration time history and is based on the effective stress method using two-dimensional FEM. The merit of the EFFCTD program lies in its usefulness in modeling embankment-ground structures subjected to liquefaction under plane strain conditions. The demerit of the EFFCTD program is that it cannot handle structures in three-dimensional conditions. Nor can it simulate the dynamic behavior of input motions with two horizontal motions.

The equation of motion for a multidimensional system is expressed by the following Eqs. (1a), (1b), and (1c).

$$\mathbf{M}\ddot{\mathbf{u}} + \mathbf{C}\dot{\mathbf{u}} + \mathbf{K}\mathbf{u} = -\mathbf{M}\ddot{\mathbf{u}}_{\mathrm{BASE}} \qquad (1a)$$

$$\sigma = \mathbf{D}\ \varepsilon \qquad (1b)$$

$$\mathbf{K}\mathbf{u} = \int_v \mathbf{B}^{\mathrm{T}}\sigma\,\mathrm{dv} \qquad (1c)$$

Where the matrices **M**, **C**, and **K** are known as an assembled mass, damping, and stiffness matrix, respectively. The vectors $\ddot{\mathbf{u}}$, $\dot{\mathbf{u}}$, $\mathbf{u}$, and $\ddot{\mathbf{u}}_{\mathrm{BASE}}$ are known as relative acceleration amplitude, velocity, displacement, and the input acceleration at base, respectively. σ is the stress vector, **D** is the elasticity matrix, ε is the strain vector, **B** is the strain shape function matrix. The EFFCTD program is based on the integration of the lumped mass matrix, the Rayleigh damping matrix, and the stiffness matrix using the incremental relation analysis. Three types of time integration algorithms are integrated in this program comprising an explicit type: Central difference method for ground with seepage flow problem; an implicit type: Newmark-β method with the initial rigid method for ground with structures; and a hybrid type: Mixed explicit and implicit methods for mixed different types of structures.

This code uses the non-linear elasticity theory for a one-phase system. It is relatively simple direct non-linear method developed by combining of the hysteresis type function model (the modified Ramberg-Osgood model or the modified Hardin-Drnevich model) which is an extension of the non-linear elasticity analysis for the one-phase system with the laboratory dynamic element test systems leading to excess pore water pressure. From the previous studies[8),9)], we think that the modified R-O model better expresses the dynamic stress-strain relationship of real soils than the modified H-D model because the latter model has excessive damping estimations for large shear strain amplitudes.

The equation of modified R-O's skeleton curve can be expressed by the following Eq. (2a) and Eq. (2b).

$$\gamma = \frac{\tau}{G_0}\left(1+\alpha'\left|\frac{\tau}{\tau_f}\right|^{\beta}\right) \qquad (2a)$$

with

$$\alpha' = 2^{\beta}, \quad \beta = \frac{2\pi h_{\max}}{2-\pi h_{\max}} \qquad (2b)$$

Where τ, τ_f, γ, and G_0 are the shear stress, shear strength, shear strain, and initial shear modulus, respectively; α' and β are non-linear parameters in the modified R-O model, h_{max} is the maximum damping ratio. Equation (2b) is based on the equivalent linear method using the relationship between the scant shear modulus and the damping ratio versus the varied shear strain amplitude. Using h_{max}, G_0, and τ_f, the shear strain γ can be determined simply.

Differentiating Eq. (2a), we can determine the tangent shear modulus G_t for the incremental dynamic response, and substitute this for the elasticity matrix **D** in Eq. (1b). The branch curves of the modified R-O hysteresis loops can be determined by applying Masing's rule.

The modified R-O model is originally a one-dimensional static stress-strain relationship. For the two-dimensional problems, assuming the dynamic shear stress $\tau_{d,xy}$ and tangent shear modules $G_{t,xy}$ in the *X-Y* plane are equivalent to one dimensional shear stress τ_d and shear modules G_t. These values are installed in the static plain strain elasticity matrix **D** proposed by Clough & Woodward[10]. The matrix **D** is expressed by Eqs. (3a), (3b), and (3c).

$$\begin{Bmatrix}\Delta\sigma_x\\ \Delta\sigma_y\\ \Delta\tau_{xy}\end{Bmatrix} = \begin{bmatrix} M_B+M_S & M_B-M_S & 0\\ M_B-M_S & M_B+M_S & 0\\ 0 & 0 & M_S\end{bmatrix}\begin{Bmatrix}\Delta\varepsilon_x\\ \Delta\varepsilon_y\\ \Delta\gamma_{xy}\end{Bmatrix} \qquad (3a)$$

$$M_B = E_0 / 2(1+\nu)(1-\nu) \qquad (3b)$$

$$M_S = E_t / 2(1+\nu) \qquad (3c)$$

Where M_B is the volume elasticity term, M_S is the shear rigidity term. Eq. (3b), however, is modified by the author. In order to maintain a constant volume (elasticity value) under the undrained condition, M_B remains unchanged in the EFFCTD. E_0 is the initial Young's modulus, E_t is the dynamic tangent Young's modulus at any time step, and ν is Poisson's ratio.

The effective stress σ' under the two-dimensional plane strain condition is expressed by Eqs. (4a) and (4b).

$$\{\sigma'\} = \{\sigma\} - \{m\}u \qquad (4a)$$

with

$$\{m\} = \{1 \quad 1 \quad 0\}^T \qquad (4b)$$

Where σ is the total stress, u is the excess pore water pressure, and vector m corresponds to Kronecker's δ indicating the tensor. In order to maintain the constant total stress value against a changing pore pressure, the excess pore water pressure u_m is expressed by Eq. (5).

$$u_m = \sigma'_{mi} - \sigma'_m \qquad (5)$$

Where σ'_{mi} is the initial effective mean stress and σ'_m is the effective mean stress at any time step.

Shear modulus G_0 is expressed by Eq. (6).

$$G_0 = G_{0i}\left(\sigma'_{mi} - u_m\right)^{0.5} \qquad (6)$$

G_{0i} is the initial shear modulus under a standard initial effective mean stress σ'_{mi}.

Shear strength τ_f is expressed by Eq. (7).

$$\tau_f = C'\cos\phi' + \left(\sigma'_{mi} - u_m\right)\sin\phi' \qquad (7)$$

Where C' and ϕ' are the cohesion and the internal friction angle in term of effective stress, respectively.

From Eq. (4a) through Eq. (7), the effective mean stress σ'_m, the shear modulus G_0, and the shear strength τ_f changed by the excess pore water pressure u_m are obtained at each time step.

The modified R-O model enables the calculation of the hysteretic non-linear behavior of soil. This model, however, cannot determine excess pore water pressure buildup accompanying the negative dilatancy because it is the one-phase system.

For the purpose of liquefaction analysis, the code for evaluating the change of excess pore water pressure was added to the elasticity matrix **D** in Eq. (1b), and in addition, the code for seepage flow analysis for the pore pressure dissipate was added.

In the EFFCTD, the buildup rate of excess pore

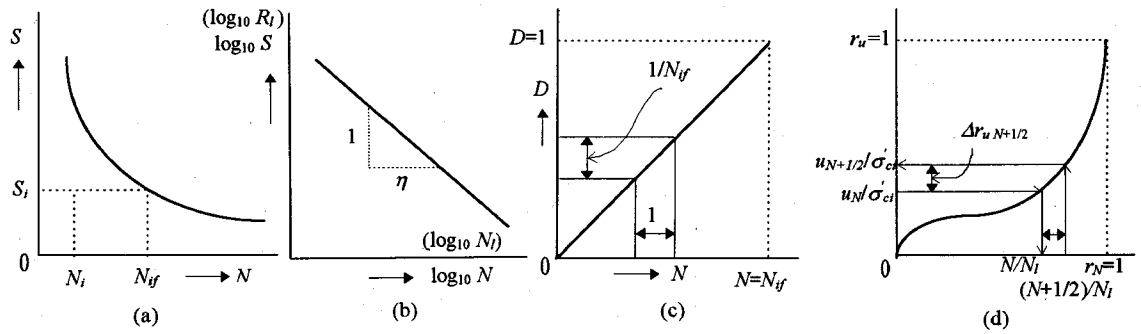

Fig. 9 Outline of liquefaction analysis in the EFFCTD

water pressure under undrained irregular shear loading has been determined by Kokusho et al.'s method[11].

Kokusho et al. established an effective stress path algorithm by using the empirical formula of excess pore water pressure buildup proposed by Seed et al.[12] and the accumulative damage concept proposed by Annaki and Lee[13].

The empirical formula by Seed is expressed by Eqs. (8a) and (8b).

$$r_N = \left[\frac{1}{2}\left(1-\cos\pi r_u\right)\right]^{\xi} \qquad (8a)$$

where

$$r_N = N/N_l, \quad r_u = u/\sigma'_{ci} \qquad (8b)$$

In which r_N is cyclic number ratio, N_l is the induced liquefaction cyclic number, r_u is the excess pore water pressure ratio, σ'_{ci} is the initial confining stress, and ξ is the Seed's empirical parameter.

Figure 9 shows an outline of liquefaction analysis in this study.

If a shear stress amplitude S_i is applied in the number of N_i in one irregular wave-form (see **Fig. 9** (a)), the damage factor D_i is expressed by the following Eq. (9a).

$$D_i = N_i / N_{if} \qquad (9a)$$

Where N_i is the cyclic number of the amplitude S_i and N_{if} is the whole number leading to damage.

When considering all shear amplitudes in the wave-form, the accumulative damage factor D is expressed by the following Eq. (9b). If D is equal to the value of 1.0, this indicates a failure condition (see **Fig. 9** (c)).

$$D = \sum_i \left(N_i / N_{if}\right) \qquad (9b)$$

To determine the irregular shear loading effects, Kokusho et al. considered the use of combination of the following three equations.

In the first, using a gradient η (= $\log_{10}\Delta N_l$ / $\log_{10}\Delta R_l$) in the full-logarithmic liquefaction resistance curve (see **Fig. 9** (b)), the relationship number of loading N_l against at 20th cycle and applied stress ratio R_l against $R_{l(20)}$ can be expressed as Eq. (10).

$$\frac{N_l}{20} = \left(\frac{R_l}{R_{l(20)}}\right)^{\eta} \qquad (10)$$

Where $R_{l(20)}$ is the liquefaction resistance factor at 20 cycles shear loading.

Second, Kokusho et al.[11] have considered the buildup in excess pore water pressure on the basis that the shear stress in case of an irregular wave pattern passes from one zero-cross to the next (half the number of the original N_i) as shown below.

$$N_i = 1/2 \qquad (11)$$

Finally, in regard to the accumulative damage factor D, it was thought that D did not show the linear relation as Eq. (9b) (see **Fig. 9** (d)). Since, then the following non-linear relation in Eq.(12) was adopted instead of Eq.(9b).

$$D = u/\sigma'_{ci} = f^{-1}\left(N/N_l\right) \qquad (12)$$

Eq. (12) should be interpreted to mean that the ratio of cyclic number vs. pore pressure buildup curve

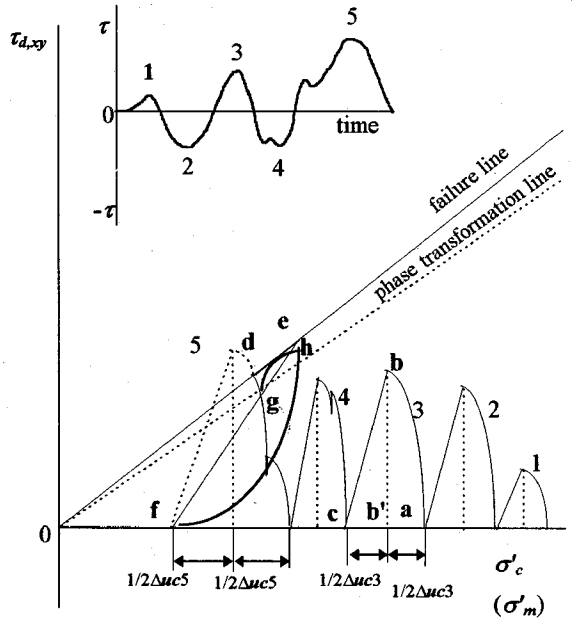

Fig. 10 Effective stress path on a stress plane

has a non-linear dependence when the accumulative damage factor shown in terms of a linear dependence is replaced by the pore pressure buildup factor.

Figure 10 shows the effective stress path on a stress plane. While the dynamic shear stress $\tau_{d,xy}$ is increasing (loading) from point a to b, the excess pore water pressure u_c increases from point a to b' based on Eq. (8a) through Eq. (12). These equations are implemented to evaluate step by step the increase in the pore pressure. On the other hand, shear stress decreases (unloading) from point b to c reversal, whereas the excess pore water pressure increases from point b' to c.

Simplified cyclic mobility effect also can be controlled on the stress plane. The effective stress path does not cross the given failure line. Once the stress path reaches the failure line under the loading (point d), the effective stress is controlled to increase along the line as long as the shear stress is being applied (from point d to e). The unloading path goes down along a straight line from point e to f. Thus, cyclic changes in the excess pore water pressure history can be simulated.

The author modified Seed et al.'s equation Eq. 8. To expand the uni-dimensional equation (Eq. 8a) to a two-dimensional expression, we have changed the confining stress σ'_{ci} to the effective mean stress σ'_{mi}. We also modified Kokusho et al.'s method partially. To achieve a better fit with the stress path obtained from the dynamic element tests, we have suitably modified the stress path curve. With the object to assess exactly the cyclic mobility effect on the stress plane, a phase transformation line, a hyperbolic curve, and a quadratic curve were added newly. When a loading path comes across the phase transformation line, it is controlled by the hyperbolic curve to approach the failure line (from point g to h). On the other side, the behavior of the unloading stress path in the cyclic mobility range follows the quadratic curve (from point h to f).

The equation of seepage flow for the two-dimensional problem is shown in the following Eq. (13).

$$\frac{\partial}{\partial x}\left(\frac{k_x}{\gamma_w}\frac{\partial u}{\partial x}\right)+\frac{\partial}{\partial y}\left(\frac{k_y}{\gamma_w}\frac{\partial u}{\partial y}\right)=m_v\left(\frac{\partial u}{\partial t}-\frac{\partial u_g}{\partial t}\right) \quad (13)$$

Where u is the total pore water pressure at any time, u_g is the dynamic excess pore water pressure, k_x and k_y are the coefficient of permeability in direction of the X and Y axis, respectively, γ_w (=ρ_w g) is the unit weight of water, and m_v is the coefficient of volume compressibility.

Using the finite element and finite difference methods, Eq. (13) can be expressed as Eq. (14).

$$\{\Delta t\theta\mathbf{A}-\mathbf{D}\}\mathbf{u}_{t+1}=-\{\Delta t(1-\theta)\mathbf{A}+\mathbf{D}\}\mathbf{u}_t - \mathbf{D}\Delta\mathbf{u}_g \quad (14)$$

Where the matrices **A** and **D** are an assembled permeability and capacity matrix, respectively. θ is the weighting coefficient which expresses the Crank-Nicolson rule when its value equals 0.5.

The results of assessment tests to evaluate the influence of the initial shear stresses were reflected the EFFCTD program developed by the author. To carry out the estimation of the excess pore water pressure (E.P.W.P.) buildup in the ground with embankment subject to the action of the initial shear stress τ_i, the results of undrained cyclic hollow cylinder torsion tests were used because of the excellent reproducibility of the anisotropic consolidated stress conditions they offer[7]. The test data were arranged so as to determine the shear stress ratio at a cyclic number N=20, that is, the cyclic shear stress ratio τ_d/σ'_{mi} and the initial shear stress ratio τ_i/σ'_{mi}, and the excess pore water pressure ratio in term of u_m/σ'_{mi}. For the Toyoura sand, the test results is shown in **Figure 11**. The solid line in **Fig. 11** stands for the contour line of the

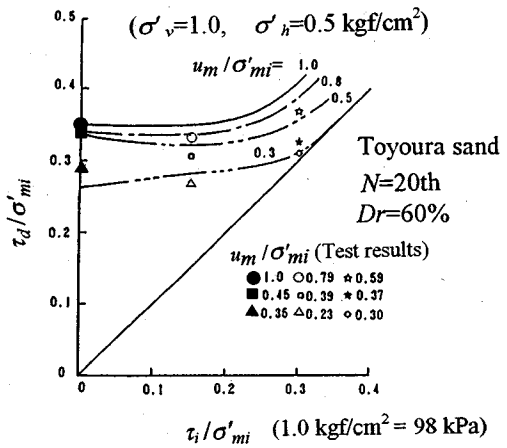

Fig. 11 Effect of the initial shear stress in the excess pore water pressure ratio changes

pore pressure that builds up, with the same number of shear cycles used as the criterion for assessment. When the relative density D_r = 60%, it was observed that the initial shear stress ratio τ_i/σ'_{mi} was 0.0, the easier it appeared for the excess pore water pressure to liquefy (u_m/σ'_{mi}=1.0) that the cyclic shear stress ratio τ_d/σ'_{mi} was nearly 0.35. However, it was found in contrast that τ_i/σ'_{mi} was more than 0.2, it became for u_m/σ'_{mi} to decrease (u_m/σ'_{mi}=0.6) that τ_d/σ'_{mi} was same value. The excess pore water pressure buildup curves of test results were incorporated into the EFFCTD program so that it became possible to reflect the effect of the initial shear stress in the maximum excess pore water pressure changes.

The program was checked against the test results quoted in the literature[9]. The outcome of these verification procedures suggest that the EFFCTD is capable of reproducing the measurement values of literature with practically complete agreement. The verification checks using the ground with embankment models[1], however, produced results differing from the measurement data for the excess pore water pressure of beneath the embankment .

(2) Refining the EFFCTD program

Using the method proposed by Fujikawa et al.[14] the authors have made improvements designed to cause any residual deformation to occur in the direction of the initial shear stress. Fujikawa et al.'s residual deformation equation is expressed by the following Eq. (15).

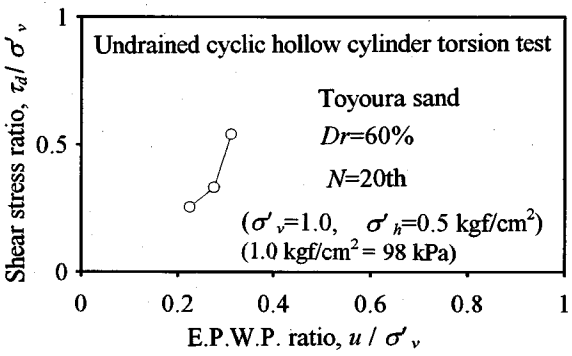

Fig. 12 Relation between shear stress ratio and E.P.W.P. ratio under lateral displacement free

$$\left.\begin{aligned} G'_0 &= G_0 / F_G \\ F_G &= 1.0 \quad (unloading: d\gamma_{xy} \cdot \gamma_{xyi} < 0.0) \\ F_G &= 1.0 + F_0 \, \gamma_{xyi} / \gamma_r \\ &(loading\ or\ reloading: d\gamma_{xy} \cdot \gamma_{xyi} > 0.0) \end{aligned}\right\} \quad (15)$$

Where G'_0 is the rectified shear rigidity at any time step, F_G is the corrective factor, F_0 is the empirical factor , γ_{xyi} is the initial shear strain, γ_{xy} is the shear strain at any time step, γ_r is the reference strain. The value F_0 of 0.1 was proposed by Fujikawa. When F_0 =0.1 was used, however, it was confirmed that the displacements obtained from the analyses are much larger than side wall displacements from the results of shaking table test . We have therefore changed F_0 =0.1 to F_0=0.001.

As mentioned above, the shaking table tests have demonstrated that there are certain areas beneath the embankment with poor lateral confinement, and to overcome this problem suitable measures have been applied to permit the calculation of the excess pore water pressure even in these areas. The effect of the presence of lateral confinement on the water pressure was investigated by the authors using dynamic element tests. Test result is shown in **Figure 12**. It can be seen that if the lateral displacement was confined, the water pressure did reach the overburden stress, whereas without this confinement, the water pressure did not reach this overburden stress. This test result was incorporated into the EFFCTD. As mentioned above stated earlier, the foot area beneath the embankment, the static analysis results have shown that the ratio of the initial effective horizontal stress σ'_{hi} to initial effective vertical stress σ'_{vi} (=K) is smaller than the coefficient of earth pressure at rest K_0. Based on this finding, we have defined a new value which is the

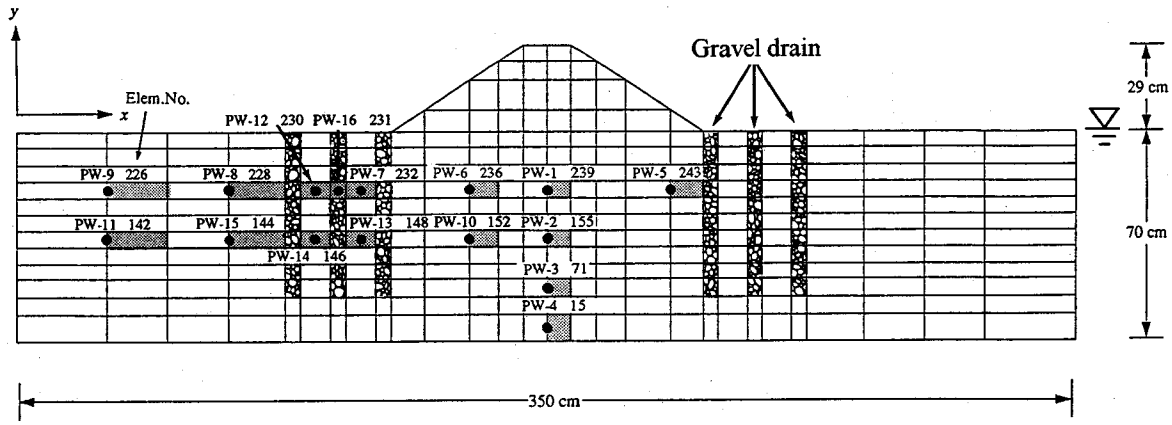

Fig. 13 Finite element model for Case-4

lateral flow factor L[15]. This factor is defined as $L=K/K_0$, and we have concluded that elements for which L assumes 1.0 or below 1.0 are finite elements with a weak lateral confining effect. The maximum E.P.W.P. value of the beneath the embankment are controlled by the method.

In the shaking table tests conducted in a 1g gravitational field, the evaluation of the liquefaction resistance stress ratio $R_{l(20)}$ always presents a problem in the ultra-low confining stress conditions near the ground surface. An advanced EFFCTD program has now been established to make such evaluation possible. The influence of the various confining stresses in the liquefaction resistance factor was investigated by Kusano[16]. Kusano's empirical formula using the dynamic tests is expressed by the following Eq. (16).

$$\left.\begin{aligned} R'_{l(20)} &= R_{l(20)} + R_4 \\ R &= -0.07 \log_{10} \sigma'_v \end{aligned}\right\} \qquad (16)$$

Where $R'_{l(20)}$ is the modified liquefaction resistance stress ratio, R_4 is the correction value for different vertical stress, σ'_v (kgf/cm^2) is the effective vertical stress. Equation (16) was useful for ultra-low confining conditions in the shaking table tests, therefore we integrated Eq. (16) in the EFFCTD program.

In order to maintain the undrained condition in the EFFCTD, we divided the Poisson's ratio ν in the Eqs. (3a) and (3b) into ν_B (for the volume elasticity term M_B) and ν_S (for the shear rigidity tram M_S).

(3) Computer procedures for EFFCTD

First, a dynamic analysis was performed using the EFFCTD in the undrained condition for the incremental time step Δt to determine the increase excess pore water pressure (E.P.W.P.) for all finite elements. Next, the E.P.W.P. values were then carried over to the seepage flow analysis in the same time step to calculate the seepage flow. The boundary conditions for this case need to be changed from the undrained condition to one corresponding to seepage flow analysis. Finally, the variation data for the pore water pressure obtained from the seepage flow analysis were then carried over once more to the dynamic analysis to perform the dynamic analysis in the step. This routine was repeated to determine the variations in pore water pressure.

(4) Analytical parameters

Figure 13 shows a finite element model for Case-4. Both components of displacements of nodes at the base were fixed. Left side displacements were set equal to right side displacements by using MPC (multi-point constrain method), because the shearing soil container was used. Analytical material parameters used in the EFFCTD are shown in **Table 1**. The parameters shown in **Table 1** are values for which the results of the static and dynamic element tests and those of the shaking table tests have been used directly and values that have been obtained indirectly from the liquefaction strength curve. In **Table 1**, G_{0i} ($= G_0 / \sigma'^{0.5}_m$, G_0: result of eigenvalue back analysis, σ'_m: the current effective mean stress) means the standard initial shear modulus with the natural frequency (e.g. 28Hz in Case-1, 30Hz in Case-2, and so on) under an effective mean stress σ'_{mi} of 1.0 gf/cm^2. h_{max} is maximum damping ratio based on dynamic deformation test results of undraiend cyclic hollow cylinder torsion test. α' and β are the R-O model's nonlinear parameters from

Table 1 Analytical parameters for EFFCTD

Materials	Unit weight γ(gf/cm^3)	Poisson's ratio ν_B	ν_S	G_{0i}(gf/cm^2) E (gf/cm^2) I (cm^4)	h_{max} (%) α' β	ϕ' (degree)	ϕ_{cm} (degree)	$R_{I\,(20)}$ σ'_{mi}= 0.5kgf/cm^2	η ξ	k_x (=k_y) (cm/sec) m_v(cm^2/gf)	Case
Ground (D_r=60%)	1.95	(0.47) 0.36	(0.30) 0.30	G_{0i}= 2.4×10^4	29 3.18, 1.67	39	28	0.165	-9.8 0.5	(2.55×10^{-2}) (2.44×10^{-4})	(Case-1), Cases-3~6
Ground (D_r=80%)	2.01	0.47	0.30	G_{0i}= 2.8×10^4	29 3.18, 1.67	45	28	0.220	-5.0 3.0	2.55×10^{-2} 2.44×10^{-4}	Case-2
Embankment	1.45	0.30	0.30	G_{0i}= 1.9×10^4	32 4.05, 2.02	39	28	-	- -	- -	Cases-1~6
Gravel drain	2.05	0.47	0.30	G_{0i}= 2.4×10^4	27 2.77, 1.47	62	28	0.330	-1.9 0.5	1.24 1.53×10^{-4}	Cases-2~4
Aluminum sheet pile	2.69	0.35	0.35	E=7.2×10^8 I=2.3×10^{-3}	-	-	-	-	- -	- -	Case-3 & Case-5
Concrete	2.30	0.17	0.17	E= 2.8×10^8	-	-	-	-	- -	- -	Case-6

exp: Cases-1,2, and 4 (Δt = 0.000125sec), imp: Cases-3,5, and 6 (Δt = 0.000415sec), Rayleigh's damping factors : α=0.0, β=0.0005

h_{max} (see Eq. 2b), respectively. ϕ' and ϕ_{cm} are the internal friction angle and the phase transformation angle, respectively. In **Table 1**, the internal friction angle for the gravel drain material has a rather large value of ϕ' = 62°. In triaxial compression test under drained condition, however, we obtained values of ϕ_d=37° and C_d = 0.15kgf/cm^2. For analysis, however, we determined the internal friction angle for which C_d becomes zero and used this internal friction angle value for our ultra-low confining analyses. Exp and imp mean the explicit and implicit time integration methods, respectively. Δt is the increment time step.

For all of shaking table tests, the author has performed simulation studies for 7 seconds from the start of vibration (half the duration of the experiments).

(5) Analytical results

The experiments and the analytical results for the seismic response acceleration amplitude and the excess pore water pressure determined from the time histories are shown in **Fig. 14 (a)** through **Fig. 14 (f)**.

From the simulation performed for the grounds including fairly loose unimproved sandy ground with embankment as in Case-1 and improved ground models as in Case-2 through Case-6, they were possible to obtain results showing the values for the

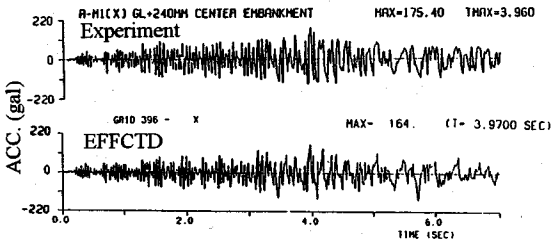

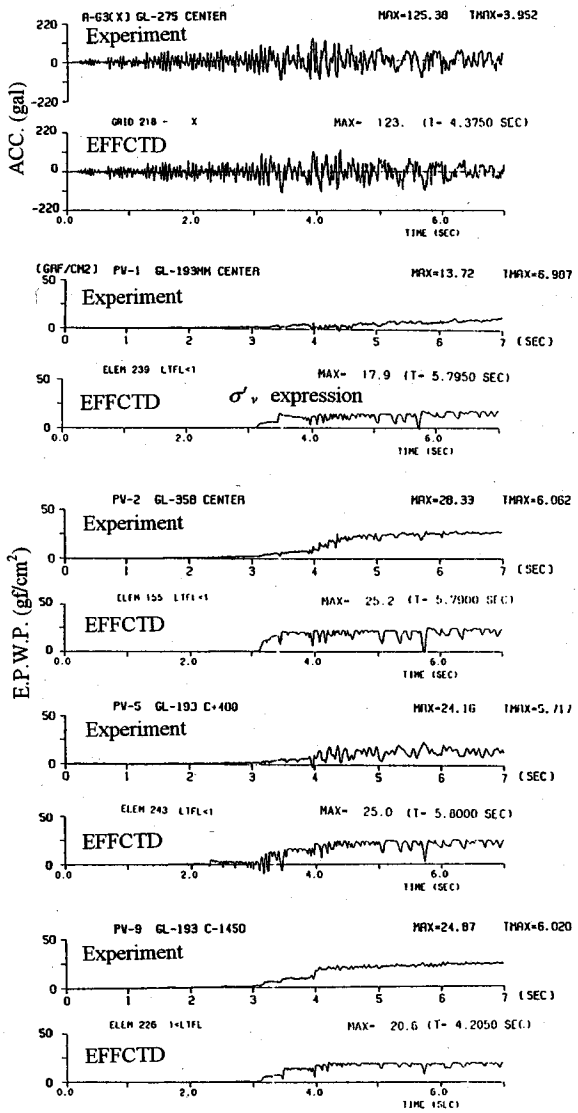

Fig. 14 (a) Comparison between experiments and analytical results (Case-1)

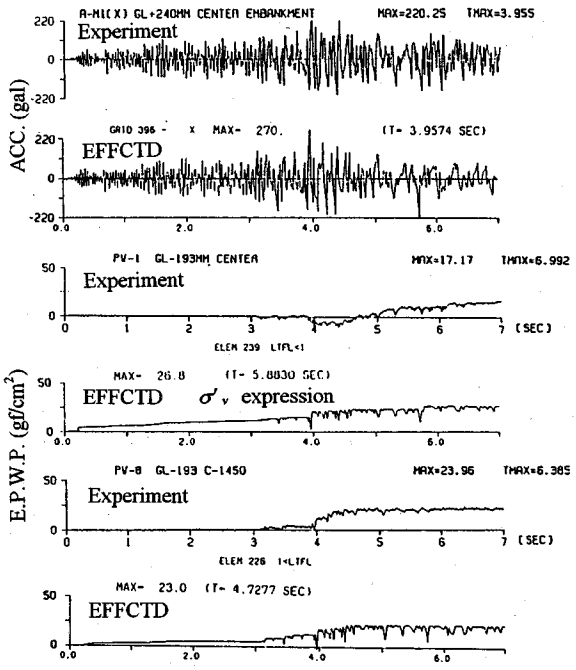

Fig. 14 (b) Comparison between experiments and analytical results (Case-2)

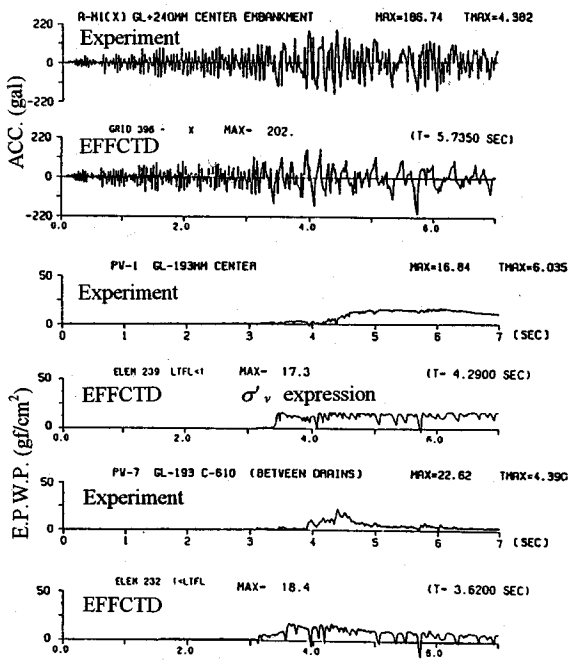

Fig. 14 (d) Comparison between experiments and analytical results (Case-4)

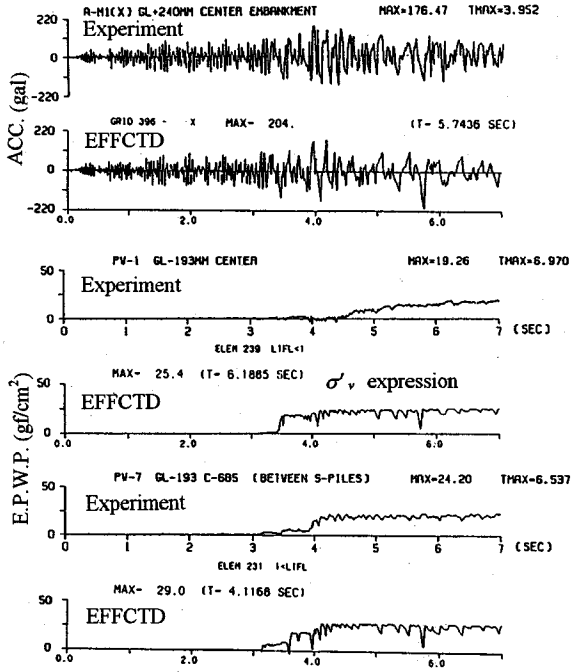

Fig. 14 (c) Comparison between experiments and analytical results (Case-3)

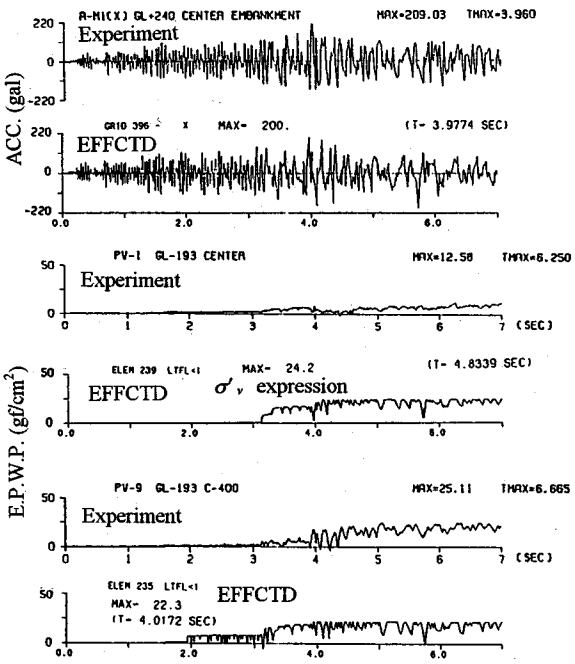

Fig. 14 (e) Comparison between experiments and analytical results (Case-5)

maximum acceleration amplitude, measured in locations such as beneath the embankment, under slope of the embankment, and on the periphery of the horizontal ground, and the analytical results were in practical agreement. The maximum excess pore water pressure values obtained from the analysis led to results that suggest general agreement with the measurement data except PW-10 in Case-6.

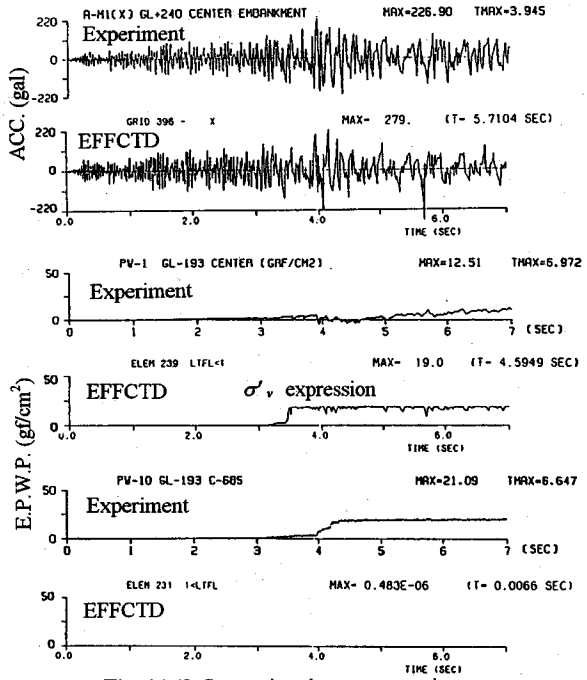

Fig. 14 (f) Comparison between experiments and analytical results (Case-6)

Especially, the substantial drop in the excess pore water pressure seen in the measurements on ground containing gravel drains of Case-4 was a reproducible phenomenon because of the seepage flow analysis code.

The lateral displacement values on the side wall of soil container obtained from all simulation models led to results that were somewhat greater than the measurement values (e.g. Experiment : EFFCTD = 0.47mm : 1.78mm at D-1 in Case-1). For the vertical displacement of the embankment crest, however, the program still failed to produce results in agreement with the measurement (e.g. EFFCTD $<$ -0.04mm at A-M1 (Y) in Case-1).

5. CONCLUSIONS

The author has developed the TOTAL system for evaluation of the seismic resistance of earth-structures taking into account the problems of soil liquefaction and have conducted research on anti-liquefaction measures adapted to the environment of the Tokyo Lowland and the static and dynamic characteristics of the ground.

From the six types of shaking table tests it can be seen that even for soft sandy ground liable to give rise to liquefaction in the surrounding horizontal ground parts, the excess pore water pressure of the foundation ground beneath the embankment does not reach the effective overburden stress and liquefaction does not occur.

While there is no liquefaction occurring in the soft sandy ground beneath the embankment, it is easy lateral flow to occur in view of the weak lateral confining so that the embankment crest shows a considerable amount of settlement.

When the toes of the embankment are symmetrically confined to prevent lateral flow, it is possible to control the amount of settlement of the embankment crest. In contrast, the improvement effect will not manifest itself easily when different improvement methods are used for the left and right sides.

When the foundation ground has been compacted, however, it is possible to control and reduce the amount of embankment crest settlement and the amount of deformation of the foundation even though there may be a high excess pore pressure. Provided that the environmental conditions for the improvement construction sites are accepted, compaction is considered to be appropriate for a particular effective anti-liquefaction method.

These simulation studies were based on the computer program EFFCTD. This program code was seen to be capable of reproducing the dynamic behavior of the foundation with embankment model in a satisfactory manner. The data obtained with this program corresponded exactly to the results obtained from experiments with the liquefaction measures and underscored effectiveness of these measures. However, the EFFCTD is incapable of reproducing the amount of vertical deformation. These results are suggesting that the reformed method is essential to forecast a post-quake deformation.

6. THEMES FOR FUTURE INVESTIGATION

To evaluate the seismic design of earth structure, it will be necessary to make a precise assessment of the amount of post seismic deformation. Attention will be focused on the deterioration in rigidity associated with the extend of liquefaction of the foundation and the foundation's progressive transition to non-linear elasticity.

Since there are limits to the reproducibility of the confining pressure in tests conducted in a 1g gravitational field, the future experimental policy will be to confirm the effectiveness of anti-liquefaction measures by using results of the centrifuge model tests which are currently being performed.

ACKNOWLEDGMENTS: The authors wish to express their thanks to Professor W.D. Liam Finn, Professor Takeji Kokusho, and Dr. Junichi Tohma for their kind and helpful advice. The authors also wish to extend their gratitude to the Ohsaki Research Institute, Inc. and Institute of Technology, the Shimizu Corporation for their support in carrying out the shaking table tests and to the CRC Research Institute, Inc. for their handling of the analytical work.

REFERENCES

1) Abe, H. : Two dimensional liquefaction analysis for ground with embankment, *Procs. of the Tenth World Conference on Earthquake Engineering*, pp.1361-1366, July, 1992.
2) Abe, H., and Kusano, K. : Shaking table tests for sandy ground with embankment, *Procs. of Fourth U.S.- Japan Workshop on Soil Liquefaction*, pp. 139-157, July,1994.
3) Abe, H., and Kusano, K. : Shaking table tests for sandy ground with embankment, *Procs. of Symposium for Waterfront Developing*, pp. 169-174, JSCE, Jan., 1992. (in Japanese)
4) Abe, H., and Kusano, K. : Shaking table tests for sandy ground with embankment, *Procs. of the Ninth Japan Earthquake Engineering Symposium 1994*, Vol.1, 895-900, Dec., 1994. (in Japanese)
5) Clough, R.W., and Pirtz, D. : Earthquake resistance of rock-fill dams, *Transaction of ASCE*, Vol.123, pp. 792-810, 1958.
6) Kurata, E., Fukuhara, T., and Noda, S : Strong-motion earthquake records on the 1983 Nipponkai-chubu earthquake in port areas, Technical Note of the Port and Harbour Research Institute, Ministry of Transport, No.458, pp. 225-259, Sept., 1983. (in Japanese)
7) Abe, H., and Kusano, K. : Measures to prevent liquefaction of embankment, *Procs. of the International Conference on Geotechnical Engineering for Coastal Development -Geocast 91-*, pp. 429-434, Sept., 1991.
8) Tazoh, T., Sato, M., Shimizu K., and Hatakeyama, A. : Nonlinear seismic response analysis of soil deposit using strong seismic records, *Procs. of Ninth World Conference on Earthquake Engineering*, pp. II 507-512, Aug., 1988.
9) Abe, H. and Kusano, K. : Two dimensional liquefaction analysis of embankment, *The 46th Japan National Conference on JSCE*, pp. III 986-987, Sept., 1991. (in Japanese)
10) Clough, R.W., and Woodward, R.J. : Analysis of embankment stresses and deformations, *Proc. ASCE*, Vol.93, SM4, pp. 529-549, 1967.
11) Kokusho, T., Esashi, Y., and Sakurai, A. : Numerical simulation on liquefaction, *CRIEPI Report*, No. 381023, 1982. (in Japanese)
12) Seed, H.B., Martin, P.P., and Lysmer, J. : Pore- water pressure changes during soil liquefaction, *Proc. ASCE*, Vol.102, GT4, pp. 323-346, 1976.
13) Annaki, M., and Lee, K.L. : Equivalent uniform cycle concept for soil dynamics, *Proc. ASCE*, Vol.103, GT6, pp. 549-564, 1977.
14) Fujikawa, S., Fukutake, K., and Ohtsuki, A. : Stress-strain relationship of soil having initial shear stress and its application to residual deformation analysis, *The 27th Japan National Conference on Soil Mechanics and Foundation Engineering*, pp. 1111-1114, July, 1992. (in Japanese)
15) Abe, H. and Kusano, K. : 2-D effective stress analysis for sandy ground with embankment, Annual Report I. C. E. of TMG, pp. 247-256, Sept., 1993. (in Japanese)
16) Kusano, K. : A method of estimating the liquefaction strength of sandy grounds containing fines, *Journal of Geotechnical engineering*, JSCE, No. 418, III-13, pp. 55 - 64, June, 1990. (in Japanese)

(Received August 28, 1995)

盛土を含む砂地盤の液状化模型振動台実験

阿部　博

緩い飽和砂地盤上にある盛土構造物の液状化時の動的挙動特性を知るために，液状化対策工を含めた合計６ケースの模型振動台実験を実施した．６つの実験に共通して，水平地盤で過剰間隙水圧が有効上載圧に達し液状化が発生しても，盛土直下の地盤では発生水圧が有効上載圧に至らないことが確認できた．一方，未改良地盤では盛土直下から斜面下で側方流動が発生しやすく，側方流動を防ぐことが液状化対策として有効であると結論した．また，非線形弾性論と液状化試験結果を組み合わせた簡便な二次元液状化解析プログラムを開発したことを述べ，振動台実験結果と解析結果との比較を行った．解析結から，残留変形量評価では課題を残したが，加振時の加速度と水圧変化には再現性があると結論した．